UNIVERSITYOF BIRMINGHAM

Synthesis, structural and magnetic characterisation of the fully fluorinated compound 6H-BaFeO$_2$F

Clemens, Oliver; Wright, Adrian; Berry, Frank; Smith, Ron; Slater, Peter

Link to publication on Research at Birmingham portal

Synthesis, structural and magnetic characterisation of the fully fluorinated compound 6H-BaFeO$_2$F

Oliver Clemens[*,a], Adrian J. Wright[a], Frank J. Berry[a], Ronald I. Smith[b], Peter R. Slater[a]

[a] School of Chemistry, University of Birmingham, Birmingham B15 2TT, United Kingdom.

[b] ISIS Facility, Rutherford Appleton Laboratory, Harwell Oxford, Didcot, OX11 0QX, United Kingdom.

*: corresponding author

Fax +44 (0)121 4144403

Email O.Clemens@bham.ac.uk

Abstract

The compound 6H-BaFeO$_2$F (P6$_3$/mmc) was synthesised by the low temperature fluorination of 6H-BaFeO$_{3-d}$ using polyvinylidenedifluoride (PVDF) as a fluorination agent. Structural characterisation by XRD and NPD suggests that the local positions of the oxygen and fluorine atoms vary with no evidence for ordering on the anion sites. This compound shows antiferromagnetic ordering at room temperature with antiparallel alignment of the magnetic moments along the c-axis. The use of PVDF also allows the possibility of tuning the fluorine content in materials of composition 6H-BaFeO$_{3-d}$F$_y$ to any value of $0 < y \leq 1$. In addition, the oxygen content, and therefore the iron oxidation state, can be tuned by applying different partial pressures of oxygen during the reaction.

1 Introduction

Perovskite type A$^{[12]}$B$^{[6]}$X$_3$ compounds are widely used for a variety of applications, such as fuel cell cathodes, solid electrolytes, and gas sensors [1-3].

In the perovskite structure, the AX$_3$ subsystem forms a close packed lattice, where the stacking sequence can differ [4] from purely cubic (c… *e. g.* for SrFeO$_2$F [5-9] and BaFeO$_2$F [7, 10-12] (both space group *Pm3m*)) to purely hexagonal (h… *e. g.* for BaCoO$_3$ [13]) and can also form lattices in between those two extremes (*e. g.* cchcch… for 6H-BaFeO$_{3-d}$ [14-19] or chcch… for 15R-BaFeO$_{3-d}$F$_{0.2}$ [20-22]). For a fully filled anion lattice X$_3$, all the B cations are octahedrally coordinated and the connection to the neighbouring octahedrons is determined from the stacking sequence. For a cation between cc layers, the octahedron is connected by corners to 6 neighbouring octahedra (3 in the layer above, 3 in the layer below) whereas for a cation between hc layers, it is connected by faces to one octahedron via the h layer and by corners to 3 octahedra via the c layer. For a cation between hh layers the connection is to 2 octahedra by faces (1 in the layer above, one in the layer below).

A range of factors can be responsible for the type of structure adopted. In addition to electronic and electrostatic reasons the average oxidation state of the B cation and therefore the relative average size of the ions, numerically expressed in the tolerance factor t [4], strongly influences the structure adopted.

The pure oxide $BaFeO_{3-d}$ can be prepared via a simple high temperature solid state reaction from the metal-oxides or -carbonates. For this system the oxygen partial pressure has been shown to be of crucial importance in determining the type of structure adopted [7, 14, 23, 24] particularly at higher temperatures. These phases and others can be fluorinated by a variety of fluorination agents [25], and prior studies have reported either a partially fluorinated $BaFeO_{3-d}F_y$ [20-22] in a 15R perovskite structure (chcch…) or fully fluorinated cubic $BaFeO_2F$ [7, 10-12] where the latter contains only Fe^{3+} and can be prepared by low temperature fluorination of the precursor oxide $BaFeO_{2.5}$ (space group $P2_1/c$, vacancy ordered distorted cubic perovskite) using PVDF.

Low temperature treatments of perovskite phases have, for many years, been known to be suitable to modify the average transition metal oxidation states and therefore allow for the synthesis of different modifications of the same product, e.g. cubic and hexagonal $SrMnO_3$ [26]. Recently, Hayashi et al. showed that cubic $BaFeO_3$ can be made by low temperature oxidation of $BaFeO_{2.5}$ ($P2_1/c$) [23]. Formation of the different modifications is supported by the good ionic conductivity of the anions, whilst the Ba/Fe substructure remains immobile at low temperatures [20]. The PVDF route [7, 25, 27] has also been shown to be a "chimie douce" route allowing the formation of kinetically stable products which decompose at higher temperatures to the thermodynamically most stable products.

The reaction mechanism for the PVDF method depends on the material which is to be fluorinated [25]. For the fluorination of $BaFeO_{2.5}$ to cubic $BaFeO_2F$, two F^- ions replace one O^{2-} ion (and the carbon residues of the polymer are burnt off by the oxygen from the air) [7, 10, 11], whereas for the fluorination of $SrFeO_3$ to cubic $SrFeO_2F$ one F^- ion replaces one O^{2-} ion (supported by the stability of the trivalent oxidation state of iron and/or the reductive potential of PVDF) [5, 6]. Hence the filling of vacancies and/or the substitution of oxygen ions are the possible reaction mechanisms for this method of fluorination (for nonstoichiometric compounds (e. g.

$Sr_{0.5}Ba_{0.5}FeO_{2.77}$ [7]) the reaction mechanism would be a combination of vacancy filling and substitution of oxygen).

Recent work has shown that perovskite phases with nearly single valent Fe^{3+} show a high stability in their magnetic ordering even at elevated temperatures. $BaFeO_2F$ (space group $Pm3m$) is a G-type antiferromagnet [10] and $SrFeO_2F$ [6] also shows antiferromagnetic ordering at ambient temperature. $15R-BaFeO_{3-d}F_y$ (space group $R3m$, $0.15 \leq y \leq 0.30$) and $6H-Ba_{0.8}Sr_{0.2}FeO_{3-d}F_y$ (space group $P6_3/mmc$, $0.15 \leq y \leq 0.25$) were also shown to be antiferromagnetically ordered, where the magnetic moments align in different directions with respect to the direction along which the AX_3 layers lie [22]. All these phases show magnetic ordering above room temperature, whereas fluorine-free mixed valent $6H-BaFeO_{3-d}$ (space group $P6_3/mmc$, d ~ 0.15) orders below 130 K [16].

In this paper, we report the first synthesis of hexagonal $6H-BaFeO_2F$ (space group $P6_3/mmc$) by low temperature fluorination of $6H-BaFeO_{3-y}$ using polyvinylidenedifluoride (PVDF) as a fluorination agent. We report on the characterisation of the sample by neutron diffraction and magnetic measurements as well as by high temperature XRD to investigate the thermal stability towards decomposition. We also describe preliminary results on the synthesis of partly fluorinated samples $6H-BaFeO_{3-d}F_y$ ($0 < y < 1$) and use lattice volume relationships to provide an estimation of their oxygen content (and consequent iron oxidation state).

2 Experimental

2.1 Sample synthesis

The precursor oxide $6H-BaFeO_{3-d}$ was prepared by a solid state reaction. Stoichiometric mixtures of high purity $BaCO_3$ and Fe_2O_3 powders (Sigma Aldrich, ≥ 99.9 %) were ground using a planetary ball mill (Fritsch pulverisette 7, 350 rpm, 1.33 h) and heated to 970°C for 12 h under flowing O_2. The samples were slowly cooled to room temperature (20°C/h) to increase the oxygen uptake and ensure the formation of the pure $6H-BaFeO_{3-d}$ phase and the procedure was repeated a second time.

For the preparation of the oxide fluorides of composition $BaFeO_{3-d}F_y$ (y = 0.2, 0.4, 0.8, 1), stoichiometric amounts of the as prepared $6H-BaFeO_{3-d}$ and

polyvinylidenedifluoride (PVDF) were thoroughly ground in n-pentane (for the synthesis of $BaFeO_2F$, y = 1, a 4 % excess of PVDF was used). The mixtures were then slowly heated to 370°C (20°C/h) under air and kept at this temperature for 20 h; slow heating was found to be beneficial to minimise the amount of BaF_2 impurity formed during the reaction (~ 1 wt-%). The as prepared oxide fluoride materials were subsequently heated to 370°C for 4h under flowing O_2 to allow uptake of oxygen, and hence maximise the Fe oxidation state.

Structural studies focused on the 6H-$BaFeO_2F$ phase, which was shown to be metastable and its' thermal decomposition was confirmed by studying the high temperature decomposition products arising from heating at 1000°C for 5 min in air.

2.2 Diffraction experiments

XRD patterns were recorded with a Bruker D5005 diffractometer with Bragg-Brentano geometry and a fine focus X-ray tube with Cu anode. No primary beam monochromator was attached. A PSD detector and a fixed divergence slit were used. The total scan time was 16 hours for the angular range between 5 and 140° 2θ.

High temperature XRD of 6H-$BaFeO_2F$ was performed with a Bruker D8 diffractometer with Bragg-Brentano geometry and a fine focus X-ray tube with Cu anode in a 2θ-range from 20 to 60 degrees and at temperatures between 30 and 750°C in steps of 30°C. A primary beam monochromator was attached and a LYNX eye detector and fixed divergence slit were used. The total scan time was 1 hour for the angular range between 20 and 60° 2θ for each temperature step.

Time of flight powder neutron diffraction (NPD) data were recorded on the newly-upgraded Polaris medium resolution diffractometer at the ISIS pulsed spallation source (Rutherford Appleton Laboratory, UK). 4g of 6H-BaFeO2F powder was loaded into a 8mm diameter thin-walled, cylindrical vanadium sample can and data collected at ambient temperature for 250μAh proton beam current to the ISIS target (corresponding to ~1¾ hours beamtime).

Structure refinement of both the XRD and NPD data was performed using the Rietveld method with the program TOPAS 4.2 (Bruker AXS, Karlsruhe, Germany) [28]. For the room temperature XRD data the whole 2θ-range was used, while for the NPD data only those data collected in the highest resolution backscattering detector bank (bank 5, average 2θ = 146.7º, d_{max} ~2.65Å) were used. The instrumental

intensity distribution for the X-ray data was determined empirically from a sort of fundamental parameters set [29] using a reference scan of LaB_6, and microstructural parameters were refined to adjust the peak shapes for the XRD data. For the neutron diffraction data, a modified pseudo Voigt function plus a Gaussian crystallite size function was used to model the time-of-flight dependence of the peak width. Lattice parameters were constrained to be the same for neutron and XRD data and the same positional parameters were used and refined for both data sets. Independent thermal displacement parameters were refined for each atom type, but the values for O and F were constrained to the same value. While these parameters were also constrained to be the same both for X-ray, and neutron, powder diffraction data, an additional B overall value was refined for XRD data accounting for further effects such as absorption or surface roughness. Reflections that showed a large magnetic scattering contribution were omitted for the initial crystallographic refinement. Furthermore, the intensities of the XRD and NPD patterns were normalised to values between 0 and 1 to give each pattern similar weight in the Rietveld analysis.

Refinement of the magnetic structure of $6H$-$BaFeO_2F$ was performed with the program GSAS [30, 31] using the NPD data collected in one of the Polaris low angle detector banks (bank 3, average $2\theta = 52.2^{o}$, $d_{max} \sim 7.02$Å). The magnetic contribution to the diffraction pattern was modelled by introducing a second phase in triclinic space group $P1$ containing just Fe atoms (to allow refinement of the magnetic structure without any symmetry restrictions), and calculating only its magnetic scattering. Unit cell, atomic positions and thermal vibration parameters in this second phase were set to the refined values determined above and then fixed to ensure that the triclinic ($P1$) cell remained geometrically and symmetrically hexagonal. Different orientations of the magnetic moments were investigated, including those previously reported for similar compounds [22].

2.3 Magnetic measurements

DC susceptibility measurements were performed over the temperature range 5-300 K using a Quantum Design MPMS SQUID magnetometer. The samples were pre-cooled to 5 K in zero field (ZFC) and also in an applied field of 0.05 T (FC) and values of χ measured whilst warming in a field of 0.05T. Field-dependent DC susceptibility measurements were performed with a Quantum Design PPMS system

with the ACMS control system in DC extraction mode. Measurements were performed at 5 K between 0 and 5 T.

2.4 Mössbauer spectroscopy

The ^{57}Fe Mössbauer spectrum was recorded in constant acceleration mode using a ca. 25 mCi ^{57}Co/Rh source at 300 K.

3 Results and discussion

3.1 Structural characterisation of 6H-BaFeO$_2$F

Fluorination of the precursor oxide 6H-BaFeO$_{3-d}$ using a 4 mole-% excess of PVDF under air resulted in the formation of a fine brown powder. The ^{57}Fe Mössbauer spectrum (see Figure 1) was best fitted to three sextets consistent with a magnetically ordered material with a Néel temperature greater than 300 K. The chemical isomer shifts δ 0.41, 0.36, 0.32 ± 0.04 mm/s are consistent [32] with iron being present only as Fe^{3+} and the formation of a phase of composition 6H-BaFeO$_2$F (in combination with the evidence of a completely filled anion lattice from the evaluation of neutron diffraction data reported later in this article).
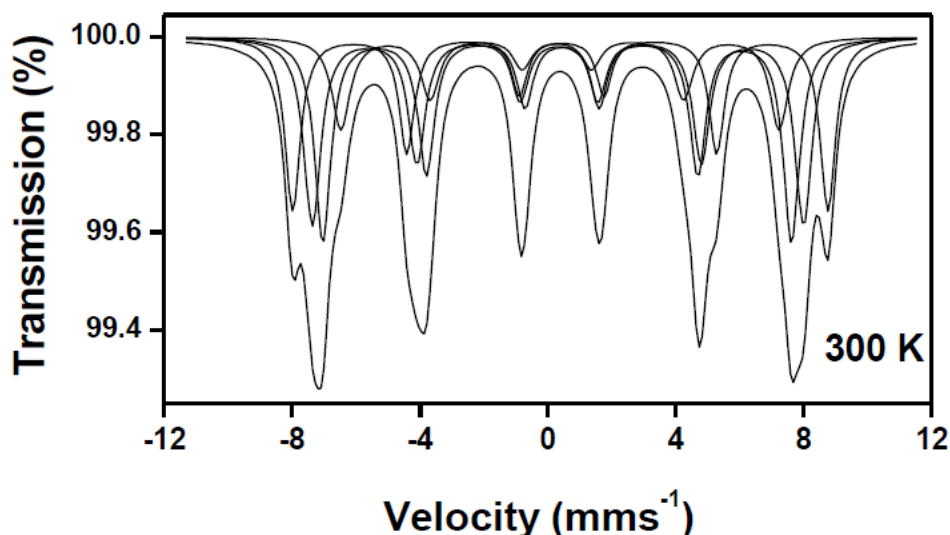
Figure 1. ^{57}Fe Mössbauer spectrum recorded at 300 K from 6H-BaFeO$_2$F. Highly fluorinated perovskite phases are known to decompose at high temperatures [7, 9]. This results from the high thermodynamic stability of the alkaline earth (AE) fluorides (AE)F$_2$ [25] and is well known for AE, or La, containing oxide fluoride compounds. In two previous articles [7, 9], it was shown that such decomposition reactions can also be used to

confirm the sample composition. A decomposition experiment at 1000°C for 5 min showed the formation of only BaF_2 (space group *Fm3m*) and $BaFe_2O_4$ (space group *Cmc2$_1$*). A quantitative Rietveld analysis indicated molar fractions of 49.7(4) and 50.3(4) mole-% of these two phases, giving an overall composition of $Ba_{0.99}Fe_1O_2F_{0.99}$ and thereby independently confirmed the assumed composition of the sample. The decomposition of 6H-$BaFeO_2F$ is therefore very similar compared to that of cubic $BaFeO_2F$ (space group *Pm3m*) [7].

6H-$BaFeO_2F$ → 0.5 BaF_2 + 0.5 $BaFe_2O_4$

A detailed structural characterisation was performed by coupled Rietveld analysis of XRPD and NPD data (see Figure 2, Figure 3 and Table 1). In this case, the NPD data allow for a more detailed analysis of the anion sublattice, which was found to have only a minor influence on the observed intensities in the XRD pattern.
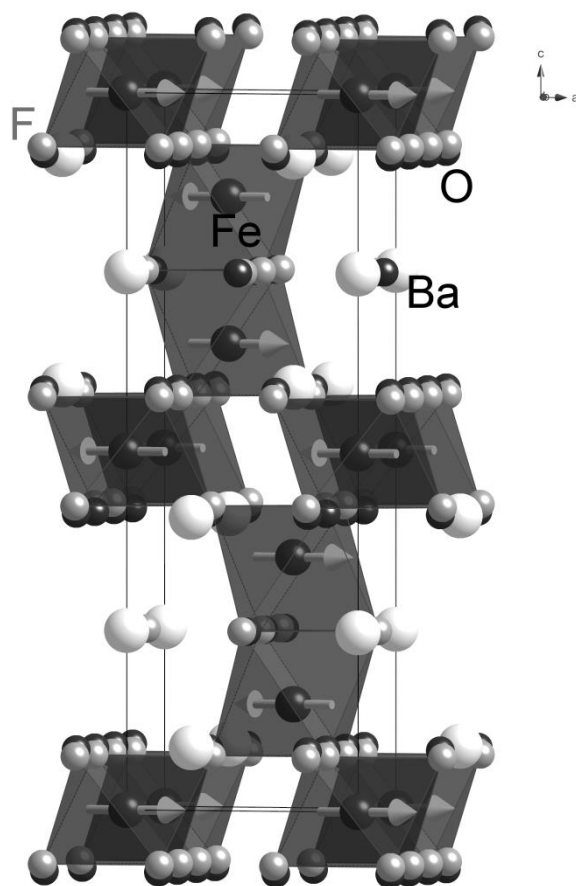

Figure 2. Refined crystal structure of hexagonal 6H-BaFeO₂F. Fluoride ions are indicated in grey and oxide ions in black. The magnetic moments on the different iron sites are indicated by arrows.

Table 1. Structural data for 6H-BaFeO₂F (space group *P6₃/mmc*) from a coupled Rietveld analysis of XRD and POLARIS bank 5 NPD data.

Atom	Wyckoff site	x	y	z	occupancy	B [Å²]
Ba^{2+}	2b	0	0	$^1/_4$	1	0.50(3)
Ba^{2+}	4f	$^1/_3$	$^2/_3$	0.08942(6)	1	0.46(2)
Fe^{3+}	2a	0	0	0	1	1.54(3)
Fe^{3+}	4f	$^1/_3$	$^2/_3$	0.85247(6)	1	1.15(3)
O^{2-}	6h	0.5148(7)	0.4852(7)	$^1/_4$	$^2/_3$	1.24(4)
O^{2-}	12k	0.1644(5)	0.8356(5)	0.5855(2)	$^2/_3$	0.79(2)
F^-	6h	0.498(1)	0.502(1)	$^1/_4$	$^1/_3$	1.24(4)
F^-	12k	0.169(1)	0.831(1)	0.5756(4)	$^1/_3$	0.79(2)
a [Å]	5.76350(4)	c [Å]	14.2119(1)	V [Å³]	408.842(7)	
R_{wp} (XRD+NPD)	2.707	GOF (XRD+NPD)	2.18	R_{Bragg}	0.85 (XRD) 2.8 (NPD)	
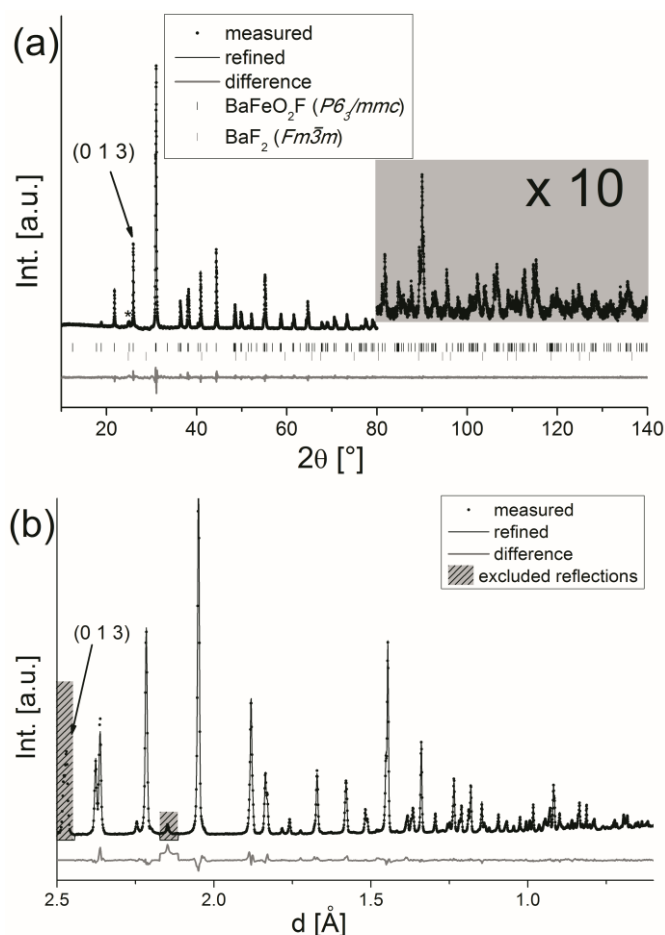
Figure 3. Coupled Rietveld analysis of XRD (a) and POLARIS bank 5 NPD (b) data from the hexagonal phase 6H-BaFeO₂F. The reflection from BaF₂ (~1.1 wt-%) with the highest intensity is marked with an asterisk for the XRD data.

Since fluorination leads to the formation of a fully occupied close packed BaO_2F sublattice, no coordination other than octahedral is obviously plausible for the Fe atoms (also confirmed by Mössbauer spectroscopy). Since no additional reflections appeared in the diffraction pattern, the same space group as for the precursor oxide $6H\text{-}BaFeO_{3\text{-}d}$ ($P6_3/mmc$) was assumed. In this space group, the anions occupy two different crystallographic sites, 6h and 12k, with the refinement indicating significant anisotropy for the thermal parameters for the anions (rod like (6h) and disk like (12k)). This led to the assumption that a model involving split positions might be more appropriate than a situation in which oxygen and fluorine occupy exactly same crystallographic positions. This is also supported by a simple consideration of their ionic radii [33], which differ by approximately 0.07 Å and therefore we might expect the local positioning of these anions to be non-identical. Indeed, initial experimental evidence for the possible correctness of this assertion was found by Rietveld analysis, where the occupancies of the split sites were allowed to refine and resulted

in values of approximately $^2/_3$ and $^1/_3$, which are consistent with the occupancies expected for O and F respectively. In the final refinement, the occupancies of the anion sites were therefore fixed to the values of $^1/_3$ for F^- and $^2/_3$ for O^{2-}, as expected from the composition and the sites assigned accordingly. Nevertheless, anisotropic parameters might also be a possible model since the difference in R_{wp} values is small (2.723 with 90 refined parameters for anisotropic displacement parameters for the anions vs. 2.707 with 85 refined parameters for split sites).

Although previously reported for the lower F content phase 6H-$Ba_{0.8}Sr_{0.2}FeO_{3-d}F_y$ (0.15 ≤ y ≤ 0.25, prepared by high temperature synthesis) [20, 22] we could not find clear evidence that the fluorine atoms favour one of the two independent crystallographic sites (6h and 12k) over the other. This also becomes apparent from calculations of the anion charges using Pauling's second rule [4] which show that for single valence Fe^{3+} and a composition $BaFeO_2F$ both anion sites 6h and 12k should have the same overall charge of $-^5/_3$ (= (-2)$*^2/_3$ + (-1)$*^1/_3$). It should also be noted that bond valence sums [34] give similar results for an ordered, as compared with a random distribution of the anions. This is consistent with iron in 6H-$BaFeO_2F$ being present as only Fe^{3+} (compared to mixed valent Fe^{3+}/Fe^{4+} in 6H-$Ba_{0.8}Sr_{0.2}FeO_{3-d}F_y$ [20, 22]).

A detailed interpretation of the split anion sites is very difficult, since the closer approach of each anion to one of the cations would increase the distance to another cation. However, a tentative assignment of the F and O atoms to these split sites (according to their occupancies) gives the refined cation-anion distances that are listed in Table 2. Importantly, the average Fe-O/F distances are 2.028 Å for the 2a and 4f sites and this compares very well with expectations based on the ionic radii (2.022 Å) [33] or from the situation in cubic $BaFeO_2F$ (2.028 Å) [7]. Furthermore, the Fe^{3+} on the 4f site is displaced from the centre of the octahedron as a result from the cation repulsion in face sharing octahedra.

Table 2. Refined cation-anion distances from a coupled Rietveld analysis of XRD and POLARIS bank 5 (backscattering) NPD data. Assignment of O^{2-} and F^- to the split positions was made according to the occupancies for the split sites.

cation-anion distances [Å]	O^{2-} (6h site)	F^- (6h site)	O^{2-} (12k site)	F^- (12k site)
Ba^{2+} (2b site)	6x 2.8856(5)	6x 2.8818(3)	6x 2.857(4)	6x 2.998(7)

|				
Ba^{2+} (4f site)	3x 2.914(4)	3x 2.814(7)	6x 2.8824(1) 3x 3.003(4)	3x 2.862(7) 6x 2.8885(4)
Fe^{3+} (2a site)	-	-	6x 2.042(4)	6x 2.000(9)
Fe^{3+} (4f site)	3x 2.102 (3)	3x 2.225 (6)	3x 1.903(4)	3x 1.933(7)

3.2 Magnetic characterisation

3.2.1 SQUID measurements

The variation of magnetic susceptibility χ (in an applied field of 0.05 T) with increasing temperature from 5 to 300 K following pre-cooling in (i) zero applied field (ZFC) and (ii) an applied field of 0.1 T (FC) is shown in Figure 4.

A divergence in the susceptibility between FC and ZFC measurements is evident over the whole temperature range and indicates a very weak ferromagnetic component. The evaluation of the field dependency of the magnetisation at 5 K is shown in Figure 5. The small magnetic moment per $6H\text{-}BaFeO_2F$ formula unit clearly indicates an antiferromagnetic ordering of the magnetic moments on the iron ions (for a detailed analysis of the magnetic structure, see section 3.2.2). Furthermore the material shows a slight hysteresis ($H_c \sim 0.2T$). The remanent magnetisation per iron ion is very low and can be estimated to be around 0.0025 μ_B. Such a magnetic moment could arise either by the presence of very small amounts of impurity phases or by a weak canting canting angle of ca. 0.02° of the magnetic moments. Both would be outside the detection limits of the neutron diffraction experiments. Similar findings were also reported for the cubic modification of $BaFeO_2F$ [10]. It is relevant to note that the remanent magnetisation is lower by about an order of magnitude than for $6H\text{-}Ba_{0.8}Sr_{0.2}FeO_{3-d}F_x$ (0.15 ≤ x ≤ 0.25) [22] and that χ_{mol} is reduced by about two orders of magnitude as compared to the precursor oxide $6H\text{-}BaFeO_{3-d}$ [17, 18].
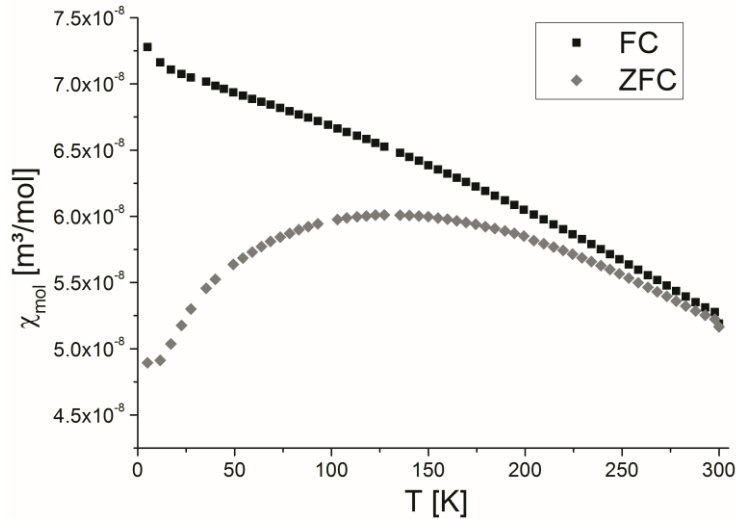
Figure 4. Variation of susceptibility χ of 6H-BaFeO₂F between 5 and 300 K. The data were recorded at increasing temperature in a measuring field of 0.05 T. Separate plots shows field cooled (FC) and zero field cooled (ZFC) data.
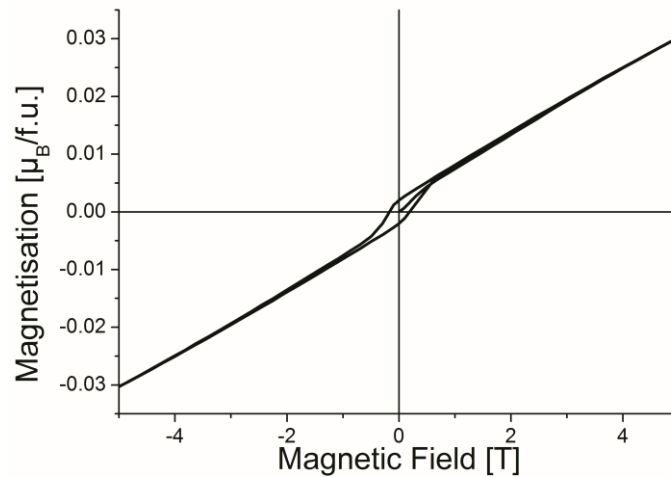
Figure 5. Field dependent magnetisation of 6H-BaFeO₂F measured at 5 K.

3.2.2 Determination of the magnetic structure

As discussed in section 3.2.1, temperature dependent measurements of the susceptibility and field dependent measurements of the magnetisation indicate an antiferromagnetic ordering of the magnetic moments. The magnetic moments are antiferromagnetically aligned in adjacent layers along the c-axis (ferromagnetically ordered in a single layer with no simple superexchange pathways between the cations in the layer). This is often found in perovskite-related materials. Strong superexchange interactions between the cations in the cc and the ch layers (~180° Fe-(O/F)-Fe angle) induces antiferromagnetism between these sites. For face shared octahedral cations in two ch layers, the Fe-(O/F)-Fe angle is close to 90°. Such

interactions favour weak ferromagnetic interactions, but direct exchange between high-spin Fe^{3+} atoms is necessarily antiferromagnetic, and the latter might therefore be the case for 6H-$BaFeO_2F$ (d(Fe_{4f}-Fe_{4f}) = 2.91 Å).

In the literature [22, 35], two models for the orientation of the magnetic moments are generally discussed: along the a- or along c-axis. A detailed analysis of bank 3 (low angle) POLARIS data reveals that, for 6H-$BaFeO_2F$, the moments align along the a-axis (resp. lie in the ab-plane) (see Figure 6a). This becomes especially evident by analysis of the reflections at ca. 4.7 Å (see inlays Figure 6a+b). Two reflections may contribute to the observed intensity of this reflection, (0 1 1) and (0 0 3), and the latter would have to carry the scattered magnetic intensity to yield a good fit. For an alignment of the magnetic moments only along c, scattered magnetic intensity would be zero for (0 0 3) [36]. The difference between these two models is also expressed in the goodness of fit for the refinements, which were significantly better when the magnetic moments were oriented along the a-axis than along the c-axis. The magnetic space group according to an alignment of the magnetic moments along the a-axis is *Cmcm* (BNS 63.457) and a subsequent refinement using this group results in an identical fit. The magnetic structure is shown in Figure 2.

The magnetic moments for the Fe^{3+} ions on the 2a and the 4f site are nearly identical (3.65(4) and 3.32(3) μ_B) being in good agreement with values observed for 6H-$Ba_{0.8}Sr_{0.2}FeO_{3-d}F_y$ (0.15 ≤ y≤ 0.25) which were slightly lower (3.56(4) and 2.72(7) μ_B) [22]. From the similarity of the magnetic moments to those of 6H-$Ba_{0.8}Sr_{0.2}FeO_{3-d}F_y$, one might expect the Néel Temperature to be similar to - or even higher than - that of 6H-$Ba_{0.8}Sr_{0.2}FeO_{3-d}F_y$ (~ around 700 K [22]). 6H-$BaFeO_2F$ therefore shows very robust antiferromagnetic ordering and T_N is expected to be of the same magnitude as reported for 6H-$Ba_{0.8}Sr_{0.2}FeO_{3-d}F_y$ (0.15 ≤ y≤ 0.25) [22], 15R-$BaFeO_{3-d}F_{y'}$ (0.15 ≤ y' ≤ 0.30) [22], cubic $BaFeO_2F$ [11] and $Sr_2Fe_2O_5$ [37].

We suggest that the exchange interaction might be different from that observed previously in the lower fluorine content 6H-$Ba_{0.8}Sr_{0.2}FeO_{3-d}F_y$ (0.15 ≤ y ≤ 0.25) [22], where a tetrahedral corner shared coordination occurs around the Fe^{3+} ions on the 4f site (caused by a shift of the anions on their positions, not by one of the Fe^{3+} ions), leading to a superexchange angle of nearly 180°. This was reported to be an additional cause of the observed robust antiferromagnetism of $Ba_{0.8}Sr_{0.2}FeO_{3-d}F_y$ (0.15 ≤ y ≤ 0.25) next to the reduction of the average iron oxidation state [22]. Since

the anion lattice is completely filled for 6H-BaFeO$_2$F only octahedral coordination can occur in this material.

It is probable that the lowering of the oxidation state helps to stabilise the antiferromagnetic ordering, as mentioned previously by Sturza et al. [22]. The Néel temperature of 6H-BaFeO$_{3-d}$ (130 K [18]) is significantly lower than that of the fluorinated compounds.
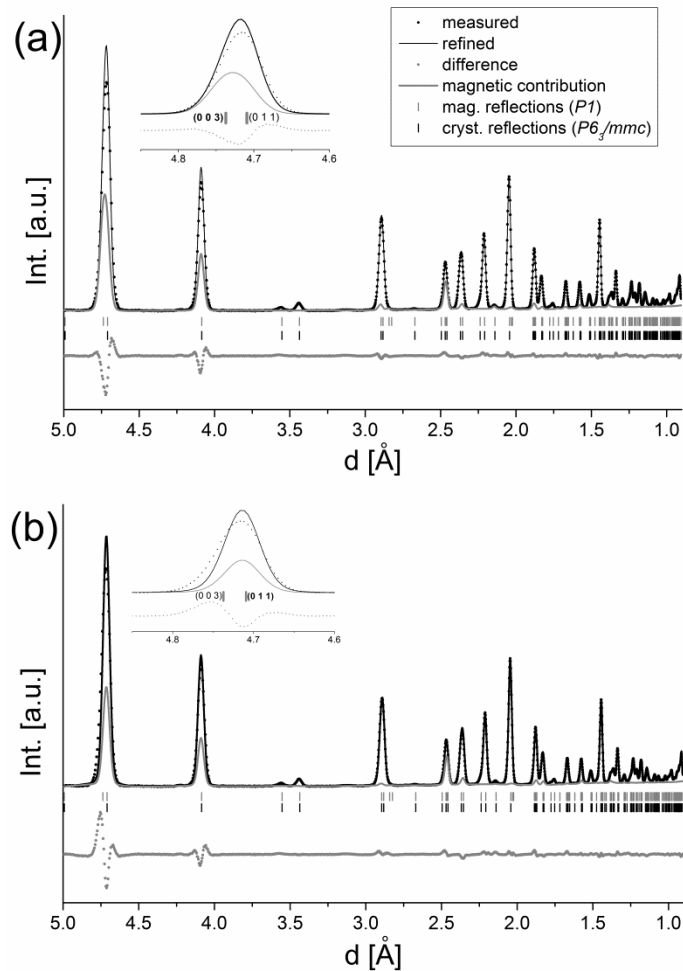
Figure 6. Rietveld analysis of POLARIS bank 3 (low angle) NPD data for different models of magnetic structures. Magnetic moments aligned parallel to the a-axis and antiferromagnetic interactions between neighbouring layers (a) and magnetic moments aligned parallel to the c-axis and antiferromagnetic interactions between neighbouring layers (b).

3.3 High temperature XRD investigations of 6H-BaFeO$_2$F

The high temperature behaviour of 6H-BaFeO$_2$F was investigated to examine the decomposition reaction in more detail. Figure 7a shows the variation of the lattice parameters (normalised to those from the lowest measurement temperature) with temperature. An almost linear relationship is observed up to ~510°C. Thereafter, the

c-lattice parameter increases greater than the a-lattice parameter and small amounts of BaF_2 begin to appear as a first decomposition product (Figure 7b). Around 700°C, the decomposition reaction seems to be complete and BaF_2 and $BaFe_2O_4$ are found in the same relative amounts as observed for full decomposition at 1000°C (see section 3.1). The fact that BaF_2 can be observed at lower temperatures than $BaFe_2O_4$ might reflect the decomposition of $BaFeO_2F$ creating a Ba/F deficient perovskite phase with formula $Ba_{1-c}FeO_2F_{1-2c}$. This could also explain why the lattice parameters a and c behave differently at temperatures higher than 510°C. The simultaneous formation of (e. g. amorphous) $BaFe_2O_4$ and BaF_2 would be expected to leave the overall composition, and therefore the nearly linear increase in lattice parameters of the hexagonal perovskite phase, largely unaffected. This is also in agreement with an attempt to refine the Ba occupancy of the partly decomposed product at ~620°C, which indicates 15 % of vacancies on the 2b site (c layer) and 5 % vacancies on the 4f site (h layer). The refined formula of $Ba_{0.92}FeO_2F_{0.84}$ is in excellent agreement with the refined weight fraction of BaF_2, again commensurate with an overall total sample composition of approximately $Ba_1Fe_{1.01}O_{2.03}F_{0.99}$. Clearly, further work will be necessary to fully understand this complex decomposition behaviour and it is planned to use this decomposition method as a synthesis route for novel A site deficient perovskites in the future.
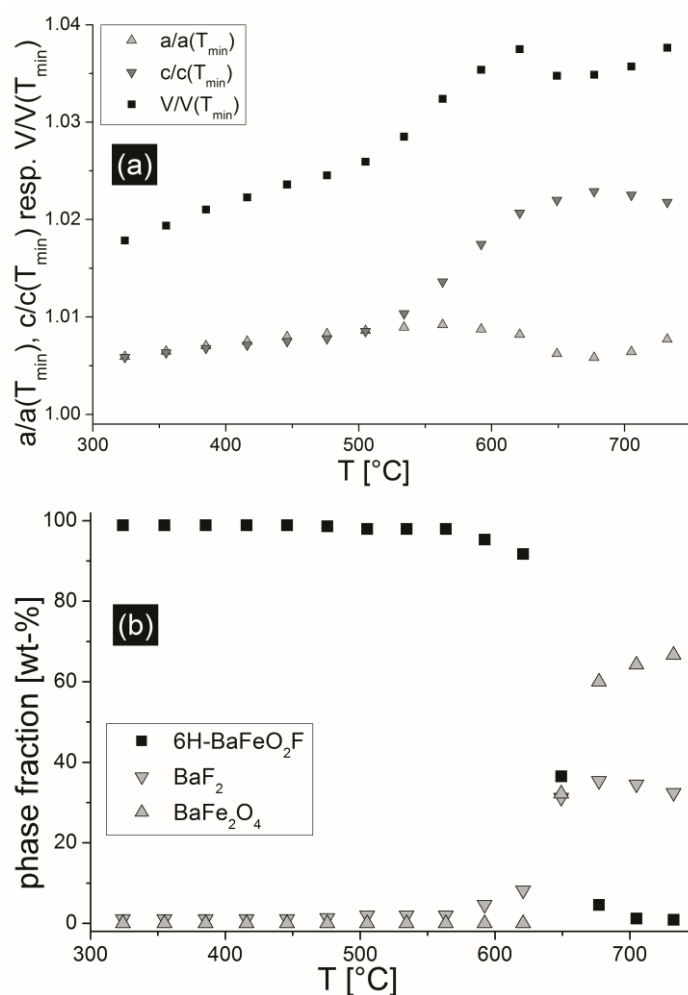
Figure 7. The high temperature behaviour of 6H-BaFeO$_2$F. Dependency of lattice parameters and cell volume (normalised to the lowest measurement temperature ~ 35°C) (a) and weight fractions of 6H-BaFeO$_2$F and its decomposition products (b).

3.4 XRD study of partly fluorinated 6H-BaFeO$_{3-d}$F$_y$

One of the key advantages in the use of PVDF as a fluorinating agent is that by varying the amount of PVDF used the fluorine content of a material can be controlled. This was illustrated in our recent fluorination studies of Sr$_3$Fe$_2$O$_{7-x}$, where a range of different phases were prepared with different fluorine contents [27]. The PVDF method also allows partial fluorination of 6H-BaFeO$_{3-d}$ leading to materials of composition 6H-BaFeO$_{3-d}$F$_y$ (see Figure 8 for XRD powder patterns). In contrast, high temperature preparations of 6H-Ba$_{0.8}$Sr$_{0.2}$FeO$_{3-d}$F$_y$ from BaF$_2$, BaCO$_3$, SrCO$_3$ and Fe$_2$O$_3$ are only suitable for a narrow range of fluorine content [20-22], due to the low thermal stability of phases with higher F contents.
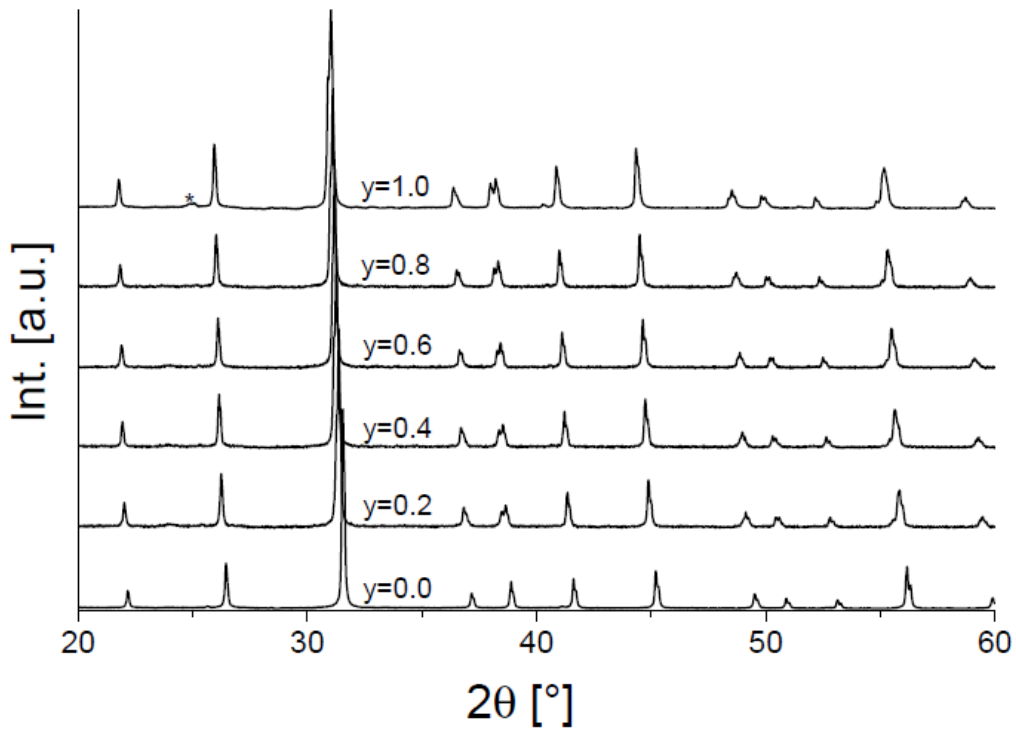
Figure 8. XRD diffraction data for samples of composition 6H-BaFeO$_{3-d}$F$_y$ (after treatment under O$_2$ atmosphere). The most intense reflection of the impurity phase BaF$_2$ (~ 1 wt-%) found for 6H-BaFeO$_2$F is marked with an asterisk.

In previous studies [7, 9], we showed that the oxidation of Fe^{3+} has the main influence on the observed cell volume. Therefore, the cell volume (see Figure 9) can be used to roughly estimate the average oxidation state of the iron species. From this, the value of d in 6H-BaFeO$_{3-d}$F$_y$ (resp. the composition of the anion lattice) can be approximated, assuming complete incorporation of F$^-$ from the PVDF (which is likely since the material can be fully fluorinated using only a very slight excess of F$^-$ in the polymer). This furthermore assumes a composition of 6H-BaFeO$_{2.81}$ for the pure oxide, as determined from our earlier titration experiments [7] and which is also in good agreement with other values from the literature [22] and a composition of 6H-BaFeO$_2$F for the fully fluorinated material, as shown by the combination of neutron diffraction, Mössbauer studies and decomposition experiments. It is also relevant to note that the cell volume of cubic BaFeO$_3$ (62.621 Å^3, Fe^{4+} only [23]) is in good agreement with that (61.899 Å^3) from the volumes and average iron oxidation states of 6H-BaFeO$_{2.81}$ and 6H-BaFeO$_2$F and therefore independently confirms the

approximate   validity   of   these   assumptions   [23].
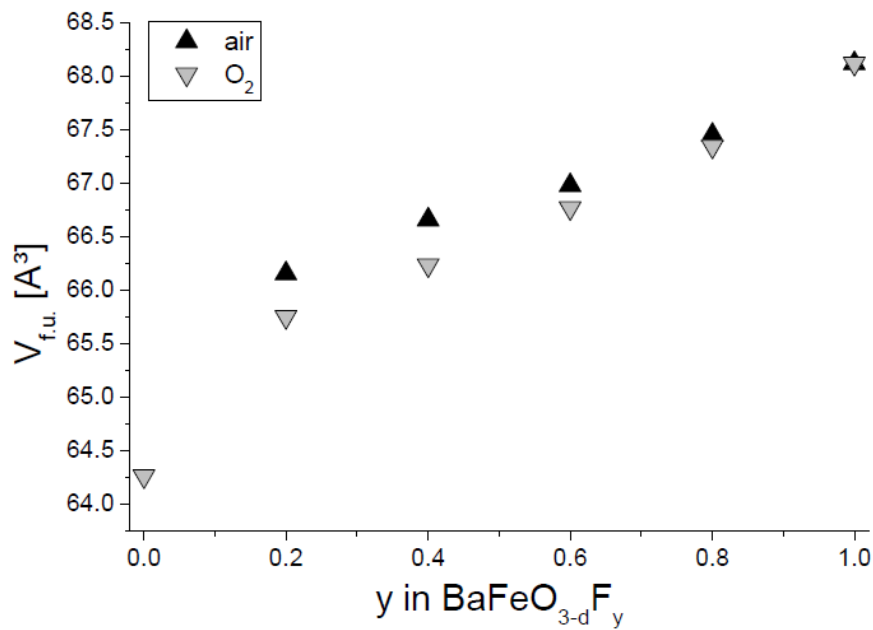

Figure 9. Dependency of the volume per BaFeO$_{3-d}$F$_y$ unit on the value of y (assuming complete F incorporation).

Values for the average iron oxidation state as well as the calculated overall composition for samples prepared under air and subsequently heated under O$_2$ are shown in Table 3. The incorporation of even low amounts of fluorine (y = 0.2) drastically lowers the iron oxidation state, with the change estimated from the cell volume being from 3.62 → 3.32. This is in agreement with the work by Sturza et al. [22], who showed that their lower F content materials 6H-Ba$_{0.8}$Sr$_{0.2}$FeO$_{3-d}$F$_y$ (0.15 ≤ y ≤ 0.25) also displayed a significantly lower oxidation state than the pure oxide (although it should be recognised that their samples were quenched from higher temperatures, which is beneficial for stabilising lower Fe oxidation states). Heating in oxygen at 370°C can only establish a marginally higher oxidation state for the Fe ions (Δq ~ 0.01 - 0.06), while the low fluoride-containing samples can be oxidised to higher degrees (as illustrated by the greater difference between air/O$_2$ points at low F contents in Figure 9). For fully fluorinated 6H-BaFeO$_2$F no significant change in the refined lattice parameters was observed and this is in agreement with a completely filled anion sublattice. Although it should be emphasised that this is an approximate approach, the results presented here suggest that low temperature F$^-$ incorporation helps stabilise the iron oxidation states closer to 3+ in the 6H perovskite structure. Such low oxidation states cannot be stabilised without destabilising the structure for the pure oxide 6H-BaFeO$_{3-d}$ (6H-BaFeO$_{3-d}$ began to decompose when

heated under air at 370°C). Further investigations by neutron diffraction are planned to investigate the influence of the fluorine content (and total anion content) on the structure and magnetic ordering in this system.

Table 3. Refined cell volumes per $BaFeX_{3-z}$ unit and approximated average iron oxidation states and material compositions for fluorinated samples $6H-BaFeO_{3-d}F_y$ (from an analysis of the cell volumes assuming complete incorporation of the F^- ions from the PVDF fluorinating agent). * The sample started to transform/decompose when heated at 370°C under air).

Fluorine content y	$V_{f.u.}$ [Å³]	Estimated average iron oxidation state	Composition	$V (O_2)$ [Å³]	Estimated average iron oxidation state	Composition
		air			O_2	
1	68.125	*3.00*	*$BaFeO_2F$*	68.123	*3.00*	*$BaFeO_2F$*
0.8	67.455	3.11	$BaFeO_{2.15}F_{0.8}$	67.349	3.12	$BaFeO_{2.16}F_{0.8}$
0.6	66.983	3.18	$BaFeO_{2.29}F_{0.6}$	66.773	3.22	$BaFeO_{2.31}F_{0.6}$
0.4	66.661	3.24	$BaFeO_{2.42}F_{0.4}$	66.238	3.30	$BaFeO_{2.45}F_{0.4}$
0.2	66.157	3.32	$BaFeO_{2.56}F_{0.2}$	65.753	3.38	$BaFeO_{2.59}F_{0.2}$
0	65.704*	-*	-*	64.264	*3.62*	*$BaFeO_{2.81}$*

4 Conclusions

We report here the first synthesis of $6H-BaFeO_2F$ by low temperature fluorination of the precursor oxide $6H-BaFeO_{3-d}$. In contrast to high temperature syntheses routes [20-22], this allows the production of a material with the highest possible fluorine content. The material decomposes at ~510°C into BaF_2 and $BaFe_2O_4$, which explains why the synthesis of this phase is not possible by high temperature reactions. $6H-BaFeO_2F$ shows robust antiferromagnetism at room temperature. Oxygen and fluorine ions are randomly distributed across the lattice, but evidence for slightly different anion positions linked to the local presence of oxygen and fluorine was found, providing different local bond distances for these anions. The PVDF method is confirmed as an excellent route to controlled fluorine contents, here allowing the preparation of $6H-BaFeO_{3-d}F_y$ ($0 < y \leq 1$) phases with different fluorine contents by simple control of the amount of PVDF used.

5 Acknowledgements

6   References

[1]   G. Deng, Y. Chen, M. Tao, C. Wu, X. Shen, H. Yang, *Electrochim. Acta* 54 (2009) 3910-3914.
[2]   P.A. Murade, V.S. Sangawar, G.N. Chaudhari, V.D. Kapse, A.U. Bajpeyee, *Curr. Appl. Phys.* 11 (2011) 451-456.
[3]   L. Nalbandian, A. Evdou, V. Zaspalis, *Int. J. Hydrogen Energy* 34 (2009) 7162-7172.
[4]   U. Müller, *Anorganische Strukturchemie*. B. G. Teubner Verlag, Wiesbaden, 2004.
[5]   F.J. Berry, X. Ren, R. Heap, P. Slater, M.F. Thomas, *Solid State Commun.* 134 (2005) 621-624.
[6]   F.J. Berry, et al., *J. Phys.: Condens. Matter* 20 (2008) 215207.
[7]   O. Clemens, R. Haberkorn, P.R. Slater, H.P. Beck, *Solid State Sci.* 12 (2010) 1455-1463.
[8]   E. Sullivan, C. Greaves, *Mater. Res. Bull.* 47 (2012) 2541-2546.
[9]   O. Clemens, M. Kuhn, R. Haberkorn, *J. Solid State Chem.* 184 (2011) 2870-2876.
[10]   F.J. Berry, F.C. Coomer, C. Hancock, Ö. Helgason, E.A. Moore, P.R. Slater, A.J. Wright, M.F. Thomas, *J. Solid State Chem.* 184 (2011) 1361-1366.
[11]   R. Heap, P.R. Slater, F.J. Berry, O. Helgason, A.J. Wright, *Solid State Commun.* 141 (2007) 467-470.
[12]   I.O. Troyanchuk, N.V. Kasper, O.S. Mantytskaya, E.F. Shapovalova, *Mater. Res. Bull.* 30 (1995) 421-425.
[13]   K. Yamaura, H.W. Zandbergen, K. Abe, R.J. Cava, *J. Solid State Chem.* 146 (1999) 96-102.
[14]   J.C. Grenier, A. Wattiaux, M. Pouchard, P. Hagenmuller, M. Parras, M. Vallet, J. Calbet, M.A. Alario-Franco, *J. Solid State Chem.* 80 (1989) 6-11.
[15]   F. Iga, Y. Nishihara, G. Kido, Y. Takeda, *J. Magn. Magn. Mater.* 104-107 (1992) 1969-1972.
[16]   F. Iga, Y. Nishihara, T. Katayama, K. Murata, Y. Takeda, *J. Magn. Magn. Mater.* 104–107, Part 3 (1992) 1973-1975.
[17]   K. Mori, T. Kamiyama, H. Kobayashi, K. Itoh, T. Otomo, S. Ikeda, *Physica B: Condensed Matter* 329–333, Part 2 (2003) 807-808.
[18]   K. Mori, T. Kamiyama, H. Kobayashi, T. Otomo, K. Nishiyama, M. Sugiyama, K. Itoh, T. Fukunaga, S. Ikeda, *J. Appl. Crystallogr.* 40 (2007) s501-s505.
[19]   M. Parras, M. Vallet-Regi, J.M. González-Calbet, J.C. Grenier, *J. Solid State Chem.* 83 (1989) 121-131.
[20]   M. Sturza, S. Daviero-Minaud, H. Kabbour, O. Gardoll, O. Mentré, *Chem. Mater.* 22 (2010) 6726-6735.
[21]   M. Sturza, S. Daviero-Minaud, M. Huvé, N. Renaut, N. Tiercelin, O. Mentré, *Inorg. Chem.* 50 (2011) 12499-12507.

[22]   M. Sturza, H. Kabbour, S. Daviero-Minaud, D. Filimonov, K. Pokholok, N. Tiercelin, F. Porcher, L. Aldon, O. Mentre, *J. Am. Chem. Soc.* 133 (2011) 10901-10909.

[23]   N. Hayashi, T. Yamamoto, H. Kageyama, M. Nishi, Y. Watanabe, T. Kawakami, Y. Matsushita, A. Fujimori, M. Takano, *Angewandte Chemie International Edition* 50 (2011) 12547-12550.

[24]   J.M. Gonzalez-Calbet, M. Parras, M. Vallet-Regi, J.C. Grenier, *J. Solid State Chem.* 86 (1990) 149-159.

[25]   P.R. Slater, *J. Fluorine Chem.* 117 (2002) 43-45.

[26]   T. Negas, R.S. Roth, *J. Solid State Chem.* 1 (1970) 409-418.

[27]   C.A. Hancock, T. Herranz, J.F. Marco, F.J. Berry, P.R. Slater, *J. Solid State Chem.* 186 (2012) 195-203.

[28]   *Topas V4.2, General profile and structure analysis software for powder diffraction data, User's Manual.* Bruker AXS, Karlsruhe, 2008.

[29]   R.W. Cheary, A.A. Coelho, J.P. Cline, *J. Res. Nat. Inst. Stand. Technol.* 109 (2004) 1-25.

[30]   A.C. Larson, R.B. Von Dreele, *Los Alamos National Laboratory Report LAUR* (1994) 86-748.

[31]   B.H. Toby, *J. Appl. Cryst.* 34 (2001) 210-213.

[32]   F. Menil, *J. Phys. Chem. Solids* 46 (1985) 763-789.

[33]   R.D. Shannon, *Acta Crystallogr.* A32 (1976) 751-767.

[34]   I.D. Brown, *The chemical bond in inorganic chemistry: the bond valence model.* Oxford University Press Inc., New York, 2002.

[35]   S.A. Ivanov, S.G. Eriksson, J. Erikssen, R. Tellgren, H. Rundlof, *Mater. Res. Bull.* 39 (2004) 615-628.

[36]   J.M.D. Coey, *Magnetism and Magnetic Materials.* Cambridge University Press, Cambridge, 2009.

[37]   M. Schmidt, S.J. Campbell, *J. Solid State Chem.* 156 (2001) 292-304.

Figure Captions

Figure 1. ^{57}Fe Mössbauer spectrum recorded at 300 K from 6H BaFeO$_2$F.

Figure 2. Refined crystal structure of hexagonal 6H BaFeO$_2$F. Fluoride ions are indicated in grey and oxide ions in black. The magnetic moments on the different iron sites are indicated by arrows.

Figure 3. Coupled Rietveld analysis of XRD (a) and POLARIS bank 5 NPD (b) data from the hexagonal phase 6H-BaFeO$_2$F. The reflection from BaF$_2$ (~1.1 wt-%) with the highest intensity is marked with an asterisk for the XRD data.

Figure 4. Variation of susceptibility χ of 6H-BaFeO$_2$F between 5 and 300 K. The data were recorded at increasing temperature in a measuring field of 0.05 T. Separate plots shows field cooled (FC) and zero field cooled (ZFC) data.

Figure 5. Field dependent magnetisation of 6H-BaFeO$_2$F measured at 5 K.

Figure 6. Rietveld analysis of POLARIS bank 3 (low angle) NPD data for different models of magnetic structures. Magnetic moments aligned parallel to the a-axis and antiferromagnetic interactions between neighbouring layers (a) and magnetic moments aligned parallel to the c-axis and antiferromagnetic interactions between neighbouring layers (b).

Figure 7. Results of the high temperature behaviour of 6H-BaFeO$_2$F. Dependency of lattice parameters and cell volume (normalized to the lowest measurement temperature ~ 35°C) (a) and weight fractions of 6H-BaFeO$_2$F and its decomposition products (b).

Figure 8. XRD diffraction data for samples of composition 6H BaFeO$_{3-d}$F$_y$ (after treatment under O$_2$ atmosphere). The most intense reflection of the impurity phase BaF$_2$ (~ 1 wt %) found for 6H-BaFeO$_2$F is marked with an asterisk.

Figure 9. Dependency of the volume per BaFeO$_{3-d}$F$_y$ unit on the value of y (assuming complete F incorporation).